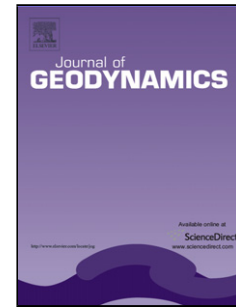


Accepted Manuscript

Title: Assessment of ground deformation following Tenerife's 2004 volcanic unrest (Canary Islands)

Authors: I. Barbero, C. Torrecillas, G. Prates, R. Páez, J. Gárate, A. García, M. Berrocoso



PII: S0264-3707(17)30138-2
DOI: <https://doi.org/10.1016/j.jog.2018.06.002>
Reference: GEOD 1579

To appear in: *Journal of Geodynamics*

Received date: 6-7-2017
Revised date: 25-2-2018
Accepted date: 17-6-2018

Please cite this article as: Barbero I, Torrecillas C, Prates G, Páez R, Gárate J, García A, Berrocoso M, Assessment of ground deformation following Tenerife's 2004 volcanic unrest (Canary Islands), *Journal of Geodynamics* (2018), <https://doi.org/10.1016/j.jog.2018.06.002>

This is a PDF file of an unedited manuscript that has been accepted for publication. As a service to our customers we are providing this early version of the manuscript. The manuscript will undergo copyediting, typesetting, and review of the resulting proof before it is published in its final form. Please note that during the production process errors may be discovered which could affect the content, and all legal disclaimers that apply to the journal pertain.

Assessment of ground deformation following Tenerife's 2004 volcanic unrest (Canary Islands)

I. Barbero (1), C. Torrecillas (2), G. Prates (1, 5), R. Páez (1, 4), J. Gárate (1), A. García (3), M. Berrocoso (1)

⁽¹⁾ Astronomy, Geodesy and Cartography Laboratory. Universidad de Cádiz, 11510 Puerto Real, Cádiz (Spain). E-mail: ignacio.barbero@uca.es

⁽²⁾ Universidad de Sevilla. Seville. Spain.

⁽³⁾ Institute of Geoscience (IGEO- CSIC/UCM)

⁽⁴⁾ Department of Statistics and Operations Research, Universidad de Cádiz.

⁽⁵⁾ UALG, Portugal.

Abstract

After the 2004 unrest on Tenerife (Canary Islands), the Global Navigation Satellite System (GNSS) network called TEGETEIDE was designed and deployed with seven survey mode stations to contribute to a volcanic alert system. Starting in 2008, public access data from continuous GNSS stations, managed by public institutions, were included in this network allowing measurement of ground displacement at 14 locations in Tenerife. Data acquired from 2005 to 2015 was analysed to assess ground deformation in Tenerife following the 2004 volcanic unrest. The overall ground deformation depicted compression in the central Las Cañadas Caldera possibly caused by gravitational subsidence of the high central volcanic cone. This sinking is generalised around the whole island but is less in the northeast (Anaga Massif) where we found an extension rate close to 200 strain/y that could be related to a secondary submarine fault accommodating rifting to the northeast and isolating the behaviour of this massif. At the south volcanic field (south rift), another localized area with an extensional deformation was detected, possibly resulting from the subsurface fluid migration or mass addition that caused the 2004 volcanic unrest because is located following the seismic swarm alignment along Icod Valley towards Roque del Conde massif that persists since that event. We also detected residual plate velocity indicating movement of Tenerife towards Gran Canaria that should be studied in the context of the entire Canary Islands archipelago.

Keywords: Ground deformation; gravitational sinking; GNSS time series; volcanic unrest; Teide

1. INTRODUCTION

Tenerife is the largest island of a volcanic complex with seven islands called the Canary Islands situated in the Atlantic Ocean close to the African passive continental margin and therefore within the Nubian tectonic plate (Figure 1). The island's active volcano is Teide, the world's third-highest volcanic structure with a height of 7,200 m from the seafloor, 3,718 m above sea level. The origin of the Canary Islands and its volcanism is still a matter of controversy with evidence for a mantle plume (Geldmacher et al. 2001; Mériaux et al. 2015), regional tectonics (Mezcua et al. 1992; Mantovani et al. 2007; Domínguez-Cerdeña et al. 2011) or a combination of both.

Volcanic activity at Teide's central phonolitic edifice, Las Cañadas Caldera (LCC), started around 3 Ma, and the caldera was formed by vertical collapses produced after intense explosive volcanic activity (Martí et al. 1997; Piña-Varas et al. 2015). The collapse scar is a preferred magma upwelling site, which likely explains the growth of Tenerife on its northern flank (Blanco-Montenegro et al. 2011). On this flank, the Teide-Pico Viejo stratovolcano complex started around 0.15 Ma. In the last 300 years, six effusive eruptions have been reported, with the last occurring in 1909. After forming the stratovolcano, the volcanic activity clustered along Tenerife's volcanic axes: NE–SW (Dorsal Rift, DR) and NW–SE (Teno-Santiago del Teide Rift, SR). These directions are in accordance with the strike of the Mid-Atlantic Ridge (MAR) and its perpendicular direction, which is reflected in Tenerife's faults (Rodríguez-Pascua et al. 2015). Furthermore, several landslides which have been or are currently active and related to the volcanic flanks can be found on Tenerife, mostly in the northern part and occurring after the caldera formation by collapses. Landslides have configured the LCC northern slope and the present morphology of northern Tenerife with the definition of the Teno, Icod, La Orotava and Anaga valleys (Ablay and Hürlimann 2000; Walter and Schmincke 2002; Hunt et al. 2011), as well as the Güimar valley in the east and some scattered areas in the south (Harris et al. 2011), see Figure 1.

The unusual increase in seismic events in 2004, with some earthquakes ($M > 3$, with depths between 0–17 km) felt by the population (Almendros et al. 2007; Domínguez-Cerdeña et al. 2011; Domínguez-Cerdeña et al. 2017), was focussed in a swarm along Icod valley towards the Roque del Conde massif (Figure 2, green dots) near Teide and has continued to this day (Figure 2, red

dots). Repeated gravity surveys revealed fluid migration, about 3-4 km of deep, from the SR to DR in the same area the seismic swarm was defined without widespread significant surface deformation (Gottsmann et al. 2006; Gottsmann et al. 2008). Before 2004, epicentres only clustered in an offshore area southeast of Tenerife, still seismically active today and associated with regional tectonic stresses (Mezcua et al. 1992; Canas et al. 1998; Romero-Ruiz et al. 2000). After the 2004 reawakening, seismic activity in Tenerife has decreased, based on the seismic station readings called CCAN (Domínguez-Cerdeña et al. 2017).

This reawakening, later reinforced by the 2011 volcanic eruption on El Hierro, the westernmost island of the Canary Islands, increased volcanic hazard awareness in the region, including a renewed interest in monitoring of ground deformation (García et al. 2014). Although previous studies of ground deformation on Tenerife were carried out between 1980 and 1990, mainly in the LCC, using classic geodesic observations, they did not detect a previous significant ground deformation (Sevilla et al. 1986; Vieira et al. 1986; Sevilla and Romero 1991; Fernández et al. 2014). In 2005, a new Global Navigation Satellite System (GNSS) network, consisting of seven survey mode GNSS stations, was designed to give support to the TEGETEIDE project whose objective is the study of the origin, evolution and consequences of the seismic activity detected in 2004 (García et al. 2006). The first results of this network, for the short period 2006–2008, detected the presence of horizontal ground displacement along a NW–SE axis, aligned with the most seismically active areas on the island and associated with the 2004 seismic unrest (NW) and tectonics (SE) (Berrocoso et al. 2010).

A combined Differential Interferometric Synthetic Aperture Radar (D-InSAR) and GNSS study carried out with data collected between 1992 and 2005, a period which included the 2004 unrest, revealed two subsiding areas, Garachico and Chío, in the northwest area of the island and around Teide (Samsonov et al. 2008), confirmed by GNSS techniques (Fernández et al. 2014); see Figure 1. These height variations were partially attributed to a decrease of the groundwater level due to water extraction in times of scarcity from some of 1052 horizontal underground galleries in Tenerife (Fernández et al. 2003; Fernández et al. 2004; Custodio et al. 2016). Subsequent D-InSAR work, using satellite images from 1992–2006, confirmed the continuation of the Chio subsidence and also revealed a general subsidence of the main island (with a value of nearly -3 mm/y in the LCC reducing to -1 mm or zero at the coastline) in opposition to the stable Anaga

massif (Fernández et al. 2014). These D-InSAR studies did not define any horizontal displacements. The last GNSS ground deformation study in Tenerife processed data from four continuous GNSS (CGNSS) stations between 2008 and 2015 (TN01, TN02, TN03 and IZAN, see Figure 1) (Sánchez-Alzola et al. 2016). Data were processed with the Precise Point Positioning (PPP) approach (Zumberge et al. 1997) revealing compression and subsidence in the central and northwest areas of Tenerife and extension in the northeast.

In this paper, we present the final result of the TEGETEIDE network confirming our previous results following shortly after 2004 unrest (only two years of GNSS campaigns and seven survey stations) (Berrocoso et al. 2010) but now with ten years of GNSS time series (2005-2015) and a greater density of GNSS stations (including ten permanent stations) such that new areas have been monitored. Horizontal velocities computed from time intervals longer than 4–5 years are sufficient to reach a velocity accuracy near 1 mm/y (Blewitt and Lavallée 2002; Bos et al. 2010), hence these new results are more accurate than the initial. A total of 17 campaign and permanent stations deployed throughout Tenerife and the surrounding islands have been processed, allowing us to explore with a higher spatial resolution the current kinematic situation and its relation to other processes mainly with volcanological or tectonic origins. Finally, clustering techniques to clean the data and strain/shear strain studies were conducted to investigate the present kinematic ground pattern of the island.

Figure 1. Schematic geological map of Tenerife Island. Rift trends: NE-SW (Dorsal Rift, DR) and NW-SE (Teno-Santiago del Teide Rift, SR). The scale bar (green to red) shows temporal changes in gravity between May 2004 and July 2005, corrected for the effect of water table changes derived from Gottsmann et al. (2006). Geological data is based on the 1:2,000,000 scale geological map of the Spanish Geology and Mining Institute (*Instituto Geológico y Minero de España*: IGME)

2. DATA

The TEGETEIDE GNSS network consists of seven campaign GNSS (cGNSS) stations (ARO1, FASN, ICOD, GUIA, OIZA, PNAL and ULLA) distributed as displayed in Figure 2. Starting in 2008, public access data from continuous GNSS (CGNSS) stations, managed by public institutions,

were included in this network. Specifically, seven stations in Tenerife: TN01, TN02, TN03, IZAN, STEI, GRAF and SNMG and three on other islands: MAS1 in Gran Canaria, LPAL in La Palma and ALAJ in La Gomera (Figure 2). Consequently, up to 17 stations could potentially be used. Created in 2016, the Canary Volcanic Institute (INVOLCA) with support from the Technological Institute of Renewable Energy (ITER), the Government of the Canary Islands and the University of Nagoya (Japan) offers a multidisciplinary vision of the monitoring of the Canary Islands (source: <http://www.involcan.org/vigilancia/red-geodesica>, February 2018). This new network includes 12 GNSS stations, 7 already existing and 5 new ones highlighting the growing interest in ground deformation monitoring in Tenerife.

Figure 2. CGNSS (black) and cGNSS (blue) stations used in this study classified by managing institution: TEGETEIDE network Spanish National Geographic Institute (IGN), EUREF Permanent Network (EUREF), Government of Canaries (GRAFCAN) and International GNSS Service (IGS). When the stations are shared between several institutions, a mixed symbol has been drawn. Dots represent seismic events in different periods (source: <http://www.ign.es/web/ign/portal/sis-catalogo-terremotos>, IGN, Feb 2018). Submarine tectonic information from Romero-Ruiz et al. (2000).

The campaign TEGETEIDE stations, cGNSS, used the same installation method and antenna fixation for every site. Permanent screws were installed as benchmarks, mounted with a stainless steel double nut to ensure accurate repeatability for every survey. Stainless steel extensors calibrated in the laboratory were attached to the benchmark permanent screws for each survey. In every campaign, the same GNSS receiver and geodetic antenna (Leica GX1230/LEIAX1200) were placed at the corresponding benchmark with the same extensor to minimise bias (Berrocoso et al. 2010). Surveys ranging in duration from three to ten days were made yearly, always in June to maintain observation conditions and prevent bias due to seasonal effects. Unfortunately, the 2011 campaign experienced some delays in the schedule so that only two of the seven benchmarks were observed, and there was no campaign in 2012. The last year of observations was 2013. To maintain homogeneity in the solution precision throughout the study, full data sets from the public CGNSS stations were included and processed taking into account some changes

in antenna devices. The date of initial data inclusion from these stations varied from 2005 to 2011. Table 1 shows the cGNSS and CGNSS stations used, their geographical coordinates in International Terrestrial Reference Frame of 2008 (ITRF2008) and initial and final dates of data.

Table 1. Geographical coordinates (ITRF2008), first and final date of data, easting, northing and vertical velocities (mm/y) with respect to the ITRF2008 reference frame with uncertainties and residuals after correction from the NNR-Morvel56 Nubia Euler pole (dV_E _Euler and dV_N _Euler) for cGNSS and CGNSS stations.

3. METHODOLOGY AND RESULTS

3.1. GNSS data processing

GNSS data were processed using Bernese software v.5.0, particularly the Bernese Processing Engine module (Dach et al. 2007) with parameters for satellite antennas igs08.atx and REPRO2 files (daily GPS orbits and GPS satellite clocks, daily GPS satellite & tracking station clocks, daily Earth rotation parameters) (Rebischung et al. 2016). A sampling rate of 30 s and a 10° elevation mask were used to minimise tropospheric refraction effects. QIF (Quasi Ionosphere-Free) algorithm was used for ambiguity resolution. Corrections for variations in Earth orientation parameters (EOP) from the International GNSS Service (IGS, <http://www.igs.org/>, February 2018) and GOT00.2 ocean tide model for Ocean Tide Load (OTL) from the Onsala Space Observatory (source: <http://holt.oso.chalmers.se/loading/>, February 2018) (Scherneck and Bos 2002) were included. Daily data sets available from MAS1 station between 2005.00 and 2016.15 were processed relative to the Rabat (RABT) CGNSS station (International GNSS Service – IGS) on the African continent. Daily station coordinates were estimated in topocentric coordinates North-East-Up (NEU). Daily time series of MAS1 relative to RABT shows that both stations move together with small residual values of about 2 mm in easting and northing (see Figure 3). Thus, MAS1 was chosen as the reference frame for Tenerife's stations.

We applied a correlation baseline strategy using the MAS1 fiducial station for the differential positioning; the reference station and precise satellite ephemerides data allowed us to compute the daily positions of the GNSS stations in the ITRF2008 reference frame. Therefore, complete

time series for each GNSS station were computed from the daily solution for all available data. The daily positioning (easting, northing and up) time series and station velocities were then computed. In order to remove outliers from the time series, a combination of a 1- σ filter after a 2- σ filter was applied, where discontinuities due to antenna changes were identified (MAS1 had two GNSS antenna changes within this study time-interval on 07-July-2008 and 18-June-2012). The topocentric coordinate velocities for each GNSS station considered offsets due to GNSS station configuration, reference frame discontinuities and antenna/receiver changes. In addition, to control other possible influences on the time series such as water table variations, STEI and TN02 residual time series were analysed. The supplementary material includes GNSS time series for every station and some residual time series.

The CGNSS station velocities were calculated using the CATS software (Williams 2008), including annual periodicities. Alternatively, for cGNSS stations, the velocities were estimated by fitting a simple linear regression model, taking into account all observed days in each campaign. Uncertainties in the estimation of the velocities have been calculated at a 95% confidence level to obtain the error ellipses (Table 1, σE and σN). These horizontal velocities contain the Nubian tectonic plate motion defined by rotation around an Euler pole. This value was subtracted from the absolute velocities of each GNSS station by the EPC Software (Goudarzi et al. 2014) using the NNR-Morvel56 tectonic model (Argus et al. 2011) with the Nubia Euler pole at 47.68° N and 68.44° W and an angular velocity of 0.292°/Ma. The horizontal velocities of GNSS stations relative to the Nubian plate were computed from 2005 to 2015; see Figure 4 and Table 1 (dVE_Euler and dVN_Euler).

Figure 3. Position time series of the MAS1 CGNSS station relative to the RABT station.

Due to the physical characteristics of the GNSS method resulting in the greatest uncertainty occurring in the vertical component (see Figure 3 Up series), we have obtained vertical velocities only for the CGNSS stations (cGNSS station data covered only ten days per campaign).

Figure 4. Residual horizontal (orange arrows) and vertical (blue arrows) velocities of GNSS stations 2005–2015 after removing the NNR-Morvel56 Euler pole for the Nubian plate. Biases

with 95% confidence level are shown as red ellipses for the horizontal and red intervals for the vertical velocities. Orthophoto basemap is from IGN (<http://pnoa.ign.es/productos> , February 2018).

3.2. Cluster analysis

A statistical cluster analysis was carried out based on the GNSS station residual horizontal velocities relative to the Nubia Euler pole rotation defined by the NNR-Morvel56 model. The goal was to find similarities among the ground displacements of the GNSS stations. The k-medoids clustering method was applied, which is a partitioning method that minimises the distance between points in a cluster and a point designated as the centre of that cluster or medoid (Kaufman and Rousseeuw 2005). It is more robust in regard to noise and outliers compared to k-means clustering because it minimises a sum of pairwise dissimilarities instead of a sum of squared Euclidean distances. This method is commonly used in domains that require robustness to outlier data, arbitrary distance metrics or for which the mean or median do not have a clear interpretation.

To determine the optimal number of k-clusters, silhouette criterion clustering was applied (Rousseeuw 1987). Silhouette is a method of interpretation and validation of consistency within cluster data. The silhouette values are a measure of how similar a point is to its own cluster compared to other clusters. The silhouette ranges from -1 to 1, where a high value indicates that the point is well matched to its own cluster and poorly matched to neighbouring clusters. This criterion suggested that the optimal number of clusters was $k=3$ (Figure 5a), with the groups shown in Figure 5b. This grouping is in agreement with the location of stations with similar kinematic behaviour, and it assigned the ULLA cGNSS station into its own cluster group, highlighting its different behaviour compared to the remaining stations. We decided to discard this campaign station in our study due to the need for an in depth study to validate its displacement, which may be caused by a local effect if we observe the behaviour of the nearest permanent station (GRAF), with the same direction but a magnitude two thirds smaller.

Figure 5. Cluster analysis. a) Grouping obtained from a cluster analysis using residual north and east velocity components from GNSS stations; b) Mean silhouette values of data grouped in one to three clusters with the maximum value for $k=3$ clusters (red point).

3.3. Strain rate computation

Strain rate computation was carried out on the whole area without any a priori subdivision because the evaluation of the velocity field highlighted that it cannot be subdivided into regions having uniform kinematics. The SSPX Software (Cardozo and Allmendinger 2009) and the grid strain package (Teza et al. 2008) were used to compute the strain rate at the nodes of a regular grid from the absolute velocities of the experimental points. We included only 12 stations, all CGNSS except OIZA (very close to IZAN and with a similar behaviour but worse precision; see Figure 4 and Table 1) and all cGNSS except ULLA (due to its anomalous behaviour according to the cluster analysis; see Figure 5b). In addition, we have included boundary conditions in a buffer of 20 km contour of the centre of the island. To this boundary, we have assigned a velocity value corresponding to the average velocity for the local reference frame in ITRF2008. The average geodetic velocity was used to define the following horizontal local reference frame: 16.1 mm/y to the east and 16.8 mm/y to the north, with a mean value module of 23 mm/y. These values are similar to our mean value for all stations in Tenerife calculated from Table 2 (16.1 ± 0.5 mm/y east, 16.5 ± 0.5 mm/y north and a velocity module 23.1 ± 0.5 mm/y). Those used in the previous TEGETEIDE study conducted by Berrocoso et al. (2010), period 2005-2008, or Martín et al. (2014) for the period 2002-2009 in the Canary Islands, are close to 25 mm/y; both studies used ITRF2005 as the reference frame and were processed with MAS1 and LPAL as fiducial stations.

For every grid node, the principal strain rates (eigenvalues of the strain rate tensor) and the corresponding directions (eigenvectors) were found. The grid resolution was set at 5 m and the Grid Distance Weighted routine was applied with a 7 km weighting factor to search for local patterns.

The strain rate field, with the principal strain rates and variations, and the shear strain rate for each grid node, where negative values indicate compression and positive values extension, are

shown in Figure 6. These results allow an evaluation of the tensional state of the crust in Tenerife. The change in area rate analysis (Figure 6b) allows the recognition of the dominant behaviour at each grid node as well as the recognition of the borders between areas characterized by different kinematics.

Figure 6. Tenerife island kinematic deformation maps: a) Strain rate field represented by extension (positive eigenvalues for main axes in blue arrows colour) and compression (negative eigenvalues for main axes in red arrows); b) Change in area rate; c) Rate of engineering shear normalized to the change in area. Black continuous line, dashed line and dotted line are represented high, medium and low significance, respectively.

4. DISCUSSION

The horizontal velocities computed for 2005 to 2015 show an average magnitude of 16.1 ± 0.5 mm/y east and 16.5 ± 0.5 mm/y north with a mean module velocity of 23.1 ± 0.5 mm/y and direction of $44.3^\circ \pm 1.3^\circ$ from south. This mean module velocity is similar to the value applied as a boundary in the strain computation (see Table 2) and the mean value of previous GNSS studies from 2002 (Berrocoso et al. 2010; Martín et al. 2014), and the direction is similar to the NNR-Morvel56 direction of 44° N in this zone (Argus et al. 2011). Rigidity and continuity seem to be two fundamental aspects of African-Nubian geodynamics with low relative velocities (Burke and Wilson 1972; Malservisi et al. 2013) and no significant (>1 mm/y) internal deformation, in agreement with the GNSS studies of McClusky and Mahmoud (2003) and Martín et al. (2014), the latter of which focussed on the current crustal deformation in the Canary Islands.

The 10-year study used all data available in the TEGETEIDE network and public stations ensuring a GPS series longer than four years and results with biases less than 1 mm/y in the velocity calculations (Blewitt and Lavallée 2002). The GNSS reference station MAS1 had two antenna changes, on 07-July-2008 and 18-June-2012, and these changes were considered. The MAS1 time series do not show special behaviour in relation to these changes, as shown in Figure 3.

After subtracting the Euler pole rotation, the overall mean trend in the horizontal residual velocities, relative to the Nubian plate and shown in Table 1 (V_E , V_N and V_U) and Figure 4, is

1.6±0.5 mm/y (in the 10-year study, the total studied deformation is around 16±5 mm) with a mean angle of -26.4±18.4° from east. This marked directionality could be a residual from the velocity of the Nubian plate, but a different calculation using mean velocities from a local reference frame obtained similar results. These displacements show a regional behaviour for Tenerife that is different from Gran Canary and which should be studied in the context of the entire archipelago to confirm crustal deformation or a relation between both islands and the submarine faults expressed by the existing seismic activity. This residual plate velocity is not shown in Sánchez-Alzola et al. (2016) because they used the PPP method in their processing and no fiducial station was used. The results of Martín et al. (2014) revealed slight velocities differences between the inner islands in the Canary Islands, obtaining a velocity value on Tenerife superior to the rest of the islands. Finally, we mention that these horizontal displacement directions do not correspond with landslide directions defined in Figure 1 even when taking into account a possible different mean plate velocity for Tenerife in the Canaries.

Continuing the velocity analysis, without taking into account the ULLA station, two main groups based on residual horizontal displacements can be identified (see Figure 5), one group with three stations in the east and the second group encompassing the rest. Focussing on the residual velocity module, the centre of Tenerife shows smaller magnitudes (~1 mm/y) in comparison with the surrounding stations, particularly stations to the west (GUIA, TN03 and STEI).

The strain rate analyses highlight different kinematics (see Figure 6) and confirm the subdivision of Tenerife into two areas with different prevailing behaviours. TN01 and GRAF, whose vectors have a direction very different from the nearby stations, seem to indicate local extension in the northeast area. In the middle of the island, lower kinematic rates induced a decrease in the extension rate from 250 to 150 strain/y that transitions to the west where the strain field changes to compression of about -60 strain/y because the western edge of Tenerife has double the kinematic rate of the middle of the island (see Figure 6a). Moving from north to south, the change in area rate (see Figure 6b) describes a decrease in the extension rate from 150 to 0 strain/y and then a change to compressional rates of about -25 strain/y for the rest of the island. In addition, near the PNAL station an area of compressional rates of -50 strain/y is observed in an area of high significance that has the same shape as the LCC and coincides with the location of a large number of seismic events that occurred from 2005 to 2016. This indicates that it is possible the

gravitational adjustment of the Teide-Pico Viejo volcanic complex, confirmed by some authors (Fernández et al. 2014; Sánchez-Alzola et al. 2016), is causing local compression in the main part of the island. In addition, the marked change from 50 strain/y to -50 strain/y in the northeast part of the island, oriented NW-SE, suggests a stable Anaga massif with the possibility of the influence of a main submarine fault helping to isolate this area (see Figure 6b). The shear strain rate field (see Figure 6c) confirms the subdivision of Tenerife into two areas with different prevailing behaviours with values of ~ 700 strain/y for the northeast and close to zero for the rest of the island.

The vertical component data shown in Table 1 (V_U) and its biases present a negative trend representing subsidence for the whole island which increases the closer one gets to the LCC. Other GNSS studies have found a decrease in elevation at GNSS stations in Tenerife since 2005 (Martín et al. 2014; Sánchez-Alzola et al. 2016), and the DInSAR study (Fernández et al. 2014) highlights the LCC with subsidence of nearly 3 mm/y but with similar values at the position of our GNSS stations (-1 or -2 mm/y). The stations located east and north of the LCC (ICOD, IZAN and OIZA) and closer to Teide have a subsidence velocity double that of stations located in the western part of the island. The stations located in the northeast (TN01 and GRAF) are the ones that show the smallest values in vertical velocities possibly due to their distance from the LCC and the influence of the submarine fault. This interpretation is based on the idea that gravitational sinking could be combined with the effect of the lowering of the water table in the island experienced during recent decades (Custodio et al. 2016) and defended by other authors (Sánchez-Alzola et al. 2016). Following the accumulated water table drawdown of Custodio et al. (2016) between 1925–1978, the ICOD and IZAN/OIZA stations are located in the region of maximum drawdown, where the horizontal water tunnel emerges in the surroundings of the LCC, and also present the maximum subsidence in our GNSS calculations. However, DinSAR studies showed significant subsidence located in small areas (Chio and Garachico) (Fernández et al. 2014) due to this process between 1996-2000. The subsidence found in this study (2005–2015) affects the whole island except the Anaga area, so it should be mainly caused by a regional effect such as the gravitational effect or isostatic adjustment of Teide. Additionally, the last DinSAR study, using ERS images up to 2005, also displays this general effect. Possible influences from water table variation in the northwest region were analysed using the STEI and TN02 time series

close to the compression area to identify periodicities related to the seasonal influence of rain, but none were found (see supplementary material res_STEI and res_TN02).

Overall, the compression of about -60 strain/y located in the central part and along the SR (Figure 6a) and the subsidence rates (see Figure 4) may be attributed to isostatic adjustment, perhaps intensified after fluid migration along the southwest margin of the LCC complex, following Gottsmann et al. (2006). The 2004 seismic swarm from Icod Valley (SR) towards the Roque del Conde massif should not be discarded due to its persistence in posterior seismic events in this area (Figure 2). Fluid pressure increase from northwest to south of the 2004 unrest zone could develop into pressure stabilization or decrease after fluid migration and therefore develop compression processes in this area (between ICOD, STEI, GUIA and PNAL).

The two patterns supported by the 2005-2015 strain map (Figure 6a) with extension in the northeast rift (DR) (coupled with low vertical velocity rates) and compression in the LCC complex (matched with increased subsidence rates) are in accordance with the results of previous geodetic data analysis and the interpretation of a central complex deflation relative to a more stable Anaga massif (Samsonov et al. 2008; Fernández et al. 2009; Tizzani et al. 2010; Sánchez-Alzola et al. 2016). Probably, this difference in behaviour between the northeast and the central block could be due to the influence of the major submarine fault (Romero-Ruiz et al. 2000; Eff-Darwich et al. 2008) defined by the high seismicity along its length (see Figure 2). In addition, both blocks are defined by a difference in the vertical velocity with stations in the north having no significant subsidence and stations in the middle of the island having higher rates of subsidence. Moreover, along the trace of the fracture from southeast to northwest there is an area rate change from 50 to -50 strain/y, as shown in Figure 6b.

CONCLUSION

The 2004 unrest on Tenerife, together with the volcanic eruption on El Hierro, resulted in risk awareness in the Canary Islands and improvement of multi-parameter observation systems for volcanic risk assessment including ground deformation monitoring. The TEGETEIDE project and GNSS network were designed with this objective. The GNSS network started with survey campaigns, but in the last few years several CGNSS stations were deployed by various institutions and incorporated into the TEGETEIDE calculations.

Survey stations increased the spatial resolution where permanent stations could not be located due to the lack of power supply, but they do not offer continuous data. The survey campaigns were careful to avoid the introduction of errors and detected differences of millimetres per year among neighbouring GNSS stations with time series containing more than 4–5 years of data. A 10-year study should offer results that are accurate enough and when the number of points is high, techniques of cluster analysis are useful to define zones with similar behaviour. In our study, we used k-medoids clustering to detect the anomalous displacement of a survey station (ULLA) and two main groups with different velocities, one in the eastern part of the island and the second encompassing the rest of the island. The marked directionality of horizontal residual velocities indicates that the regional behaviour in Tenerife is different from Gran Canaria, which should be studied in the context of the entire Canary Islands archipelago to determine whether the seismic areas between islands have any kind of influence or it is due to crustal deformation.

Additionally, strain rate maps are necessary to understand the kinematics of the island. Our computed strain rate maps depict two different kinematic areas. The first area is compatible with a gravitational sinking or isostatic adjustment, perhaps intensified after fluid migration from the northwest to the south in an alignment marked by seismicity, with gravimetric anomalies depicting compression around LCC and slight extension in the south. This first area also shows a vertical component of subsidence depicting compression of the central LCC and northwest region compatible with the distribution of area rate changes and the most recent DinSAR results. The second area is characterized by extension in the northeast rift (DR) possibly related to the action of a secondary fault that isolates the Anaga massif from the central part of the island and no subsidence due to the distance from the LCC and its sinking effect.

These results agree with the first conclusions of the TEGETEIDE network for the 2006-2008 period, showing that the kinematics of Tenerife are unchanged over the last ten years. Finally, we do not detect displacement related to landslides.

ACKNOWLEDGMENTS

This research has been partially funded by the projects TEGETEIDE (CGL2004-21643E), METOTEIDE (CGL2005-25066E), VOLRESTE (CGL2009-MEC) and PEVERTE (CGL2011-28682-C02-01) as well as the 200430E438 CSIC project. We would like to especially thanks the

participants in the TEGETEIDE campaigns, especially the members of “Laboratorio de Astronomía, Geodesia y Cartografía” of University of Cadiz, and the constructive comments of an anonymous reviewer.

ACCEPTED MANUSCRIPT

REFERENCES

- Ablay G, Hürlimann M (2000) Evolution of the north flank of Tenerife by recurrent giant landslides. *J Volcanol Geotherm Res* 103:135–159. doi: 10.1016/S0377-0273(00)00220-1
- Almendros J, Ibáñez JM, Carmona E, Zandomenighi D (2007) Array analyses of volcanic earthquakes and tremor recorded at Las Cañadas caldera (Tenerife Island, Spain) during the 2004 seismic activation of Teide volcano. *J Volcanol Geotherm Res* 160:285–299. doi: 10.1016/j.jvolgeores.2006.10.002
- Argus DF, Gordon RG, Demets C (2011) Geologically current motion of 56 plates relative to the no-net-rotation reference frame. *Geochemistry, Geophys Geosystems* 12:1–13. doi: 10.1029/2011GC003751
- Berrocoso M, Carmona J, Fernández-Ros A, et al (2010) Kinematic model for Tenerife Island (Canary Islands, Spain): Geodynamic interpretation in the Nubian plate context. *J African Earth Sci* 58:721–733. doi: 10.1016/j.jafrearsci.2010.04.007
- Blanco-Montenegro I, Nicolosi I, Pignatelli A, et al (2011) New evidence about the structure and growth of ocean island volcanoes from aeromagnetic data: The case of Tenerife, Canary Islands. *J Geophys Res Solid Earth* 116:1–17. doi: 10.1029/2010JB007646
- Blewitt G, Lavallée D (2002) Effect of annual signals on geodetic velocity. *J Geophys Res* 107:2156–2202. doi: 10.1029/2001JB000570
- Bos MS, Bastos L, Fernandes RMS (2010) The influence of seasonal signals on the estimation of the tectonic motion in short continuous GPS time-series. *J Geodyn* 49:205–209. doi: 10.1016/j.jog.2009.10.005
- Burke K., Wilson JT. (1972) Is the African Plate Stationary? *Nature* 239:387–390. doi: 10.1038/239387b0
- Canas JA, Ugalde A, Pujades LG, et al (1998) Intrinsic and scattering seismic wave attenuation in the Canary Islands. *J Geophys Res Solid Earth* 103:15037–15050. doi: 10.1029/98JB00769
- Cardozo N, Allmendinger RW (2009) SSPX: A program to compute strain from displacement/velocity data. *Comput Geosci* 35:1343–1357. doi: 10.1016/j.cageo.2008.05.008
- Custodio E, Cabrera MDC, Poncela R, et al (2016) Groundwater intensive exploitation and mining

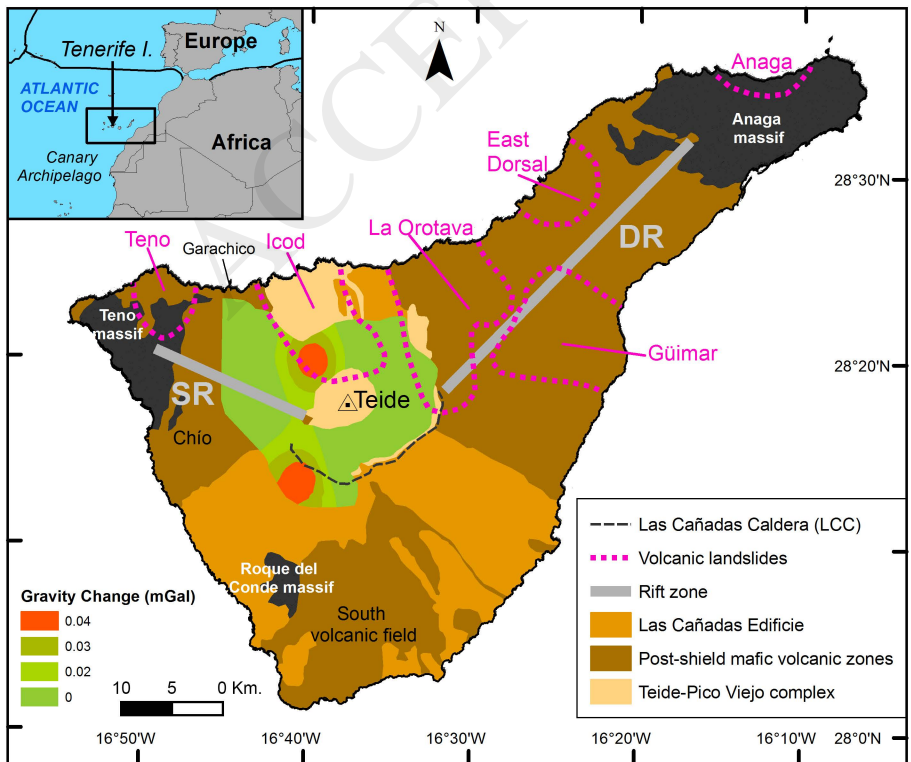
- in Gran Canaria and Tenerife, Canary Islands, Spain: Hydrogeological, environmental, economic and social aspects. *Sci Total Environ* 557–558:425–37. doi: 10.1016/j.scitotenv.2016.03.038
- Dach R, Hugentobler U, Fridez P, Meindl M (2007) Bernese GPS software version 5.0. User manual. Astronomical Institute, University of Berne
- Domínguez-Cerdeña I, del Fresno C, Cantavella J V., et al (2017) Comment on BGeochemical evidences of seismo-volcanic unrests at the NW rift-zone of Tenerife, Canary Islands, inferred from diffuse CO₂ emission[^] by Hernández P. A., Padilla G., Barrancos J., Melián G., Padrón E., Asensio-Ramos M., Rodríguez F., Pérez N.M., A. *Bull Volcanol* 80:1–4. doi: 10.1007/s00445-017-1182-0
- Domínguez-Cerdeña I, del Fresno C, Rivera L (2011) New insight on the increasing seismicity during Tenerife's 2004 volcanic reactivation. *J Volcanol Geotherm Res* 206:15–29. doi: 10.1016/j.jvolgeores.2011.06.005
- Eff-Darwich A, Grassin O, Fernández J (2008) An Upper Limit to Ground Deformation in the Island of Tenerife, Canary Islands, for the Period 1997–2006. *Pure Appl Geophys* 165:1049–1070. doi: 10.1007/s00024-008-0346-4
- Fernández J, González PJ, Camacho AG, et al (2014) An Overview of Geodetic Volcano Research in the Canary Islands. *Pure Appl Geophys*. doi: 10.1007/s00024-014-0916-6
- Fernández J, Romero R, Carrasco D, et al (2004) Detection of displacements on Tenerife Island, Canary Islands, using radar interferometry. *Geophys J Int* 160:33–45. doi: 10.1111/j.1365-246X.2005.02487.x
- Fernández J, Tizzani P, Manzo M, et al (2009) Gravity-driven deformation of Tenerife measured by InSAR time series analysis. *Geophys Res Lett* 36:L04306. doi: 10.1029/2008GL036920
- Fernández J, Yu T-T, Rodríguez-Velasco G, et al (2003) New geodetic monitoring system in the volcanic island of Tenerife, Canary Islands, Spain. Combination of InSAR and GPS techniques. *J Volcanol Geotherm Res* 124:241–253. doi: 10.1016/S0377-0273(03)00073-8
- García A, Fernández-Ros A, Berrocoso M, et al (2014) Magma displacements under insular volcanic fields, applications to eruption forecasting: El Hierro, Canary Islands, 2011–2013. *Geophys J Int* 197:322–334. doi: 10.1093/gji/ggt505
- García A, Ortiz R, Marrero JM, et al (2006) Monitoring the reawakening of Canary Islands' Teide

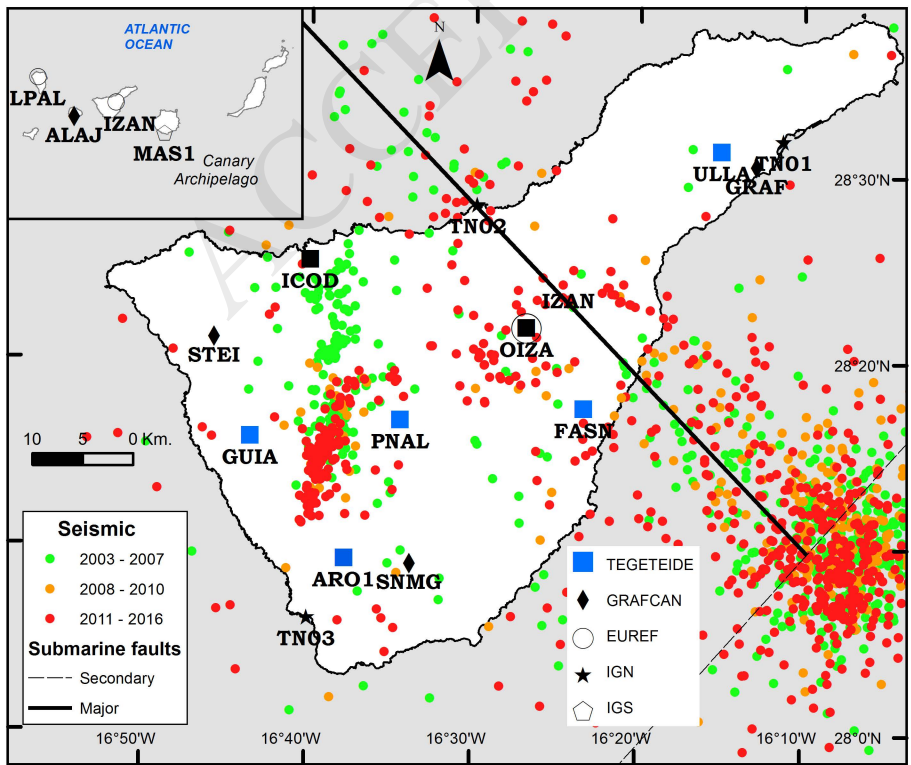
- Volcano. *Eos, Trans Am Geophys Union* 87:61. doi: 10.1029/2006EO060001
- Geldmacher J, Hoernle K, Van Den Bogaard P, et al (2001) Earlier history of the ≥ 70 -Ma-old Canary hotspot based on the temporal and geochemical evolution of the Selvagen Archipelago and neighboring seamounts in the Eastern North Atlantic. *J Volcanol Geotherm Res* 111:55–87. doi: 10.1016/S0377-0273(01)00220-7
- Gottsmann J, Camacho AG, Martí J, et al (2008) Shallow structure beneath the Central Volcanic Complex of Tenerife from new gravity data: Implications for its evolution and recent reactivation. *Phys Earth Planet Inter* 168:212–230. doi: 10.1016/j.pepi.2008.06.020
- Gottsmann J, Wooller L, Martí J, et al (2006) New evidence for the reawakening of Teide volcano. *Geophys Res Lett* 33:L20311. doi: 10.1029/2006GL027523
- Goudarzi MA, Cocard M, Santerre R (2014) EPC: Matlab software to estimate Euler pole parameters. *GPS Solut* 18:153–162. doi: 10.1007/s10291-013-0354-4
- Harris PD, Branney MJ, Storey M (2011) Large eruption-triggered ocean-island landslide at Tenerife: Onshore record and long-term effects on hazardous pyroclastic dispersal. *Geology* 39:951–954. doi: 10.1130/G31994.1
- Hunt JE, Wynn RB, Masson DG, et al (2011) Sedimentological and geochemical evidence for multistage failure of volcanic island landslides: A case study from Icod landslide on north Tenerife, Canary Islands. *Geochemistry, Geophys Geosystems* 12:1–36. doi: 10.1029/2011GC003740
- Kaufman L, Rousseeuw PJ (2005) Front Matter. In: Kaufman L, Rousseeuw PJ (eds) *Finding Groups in Data: An Introduction to Cluster Analysis*. John Wiley & Sons, Inc., Hoboken, NJ, USA, pp i–xiv
- Malservisi R, Hugentobler U, Wonnacott R, Hackl M (2013) How rigid is a rigid plate? Geodetic constraint from the TrigNet CGPS network, South Africa. *Geophys J Int* 192:918–928. doi: 10.1093/gji/ggs081
- Mantovani E, Viti M, Babbucci D, Albarello D (2007) Nubia-Eurasia kinematics: An alternative interpretation from Mediterranean and North Atlantic evidence. *Ann Geophys* 50:341–366. doi: 10.4401/ag-3073
- Martí J, Hurlimann M, Ablay GJ, Gudmundsson A (1997) Vertical and lateral collapses on Tenerife (Canary Islands) and other volcanic ocean islands. *Geology* 25:879. doi: 10.1130/0091-

7613(1997)025<0879:VALCOT>2.3.CO;2

- Martín A, Sevilla M, Zurutuza J (2014) Crustal deformation study in the Canary Archipelago by the analysis of GPS observations. *J Appl Geod*. doi: 10.1515/jag-2014-0002
- McClusky S, Mahmoud S (2003) GPS constraints on Africa and Arabi plate motions. *GeophysJInt* 155:126–138.
- Mériaux CA, Duarte JC, Duarte SS, et al (2015) Capture of the Canary mantle plume material by the Gibraltar arc mantle wedge during slab rollback. *Geophys J Int* 201:1717–1721. doi: 10.1093/gji/ggv120
- Mezcua J, Buforn E, Udías A, Rueda J (1992) Seismotectonics of the Canary Islands. *Tectonophysics* 208:447–452. doi: 10.1016/0040-1951(92)90440-H
- Piña-Varas P, Ledo J, Queralt P, et al (2015) Vertical collapse origin of Las Cañadas caldera (Tenerife, Canary Islands) revealed by 3-D magnetotelluric inversion. *Geophys Res Lett* 42:1710–1716. doi: 10.1002/2015GL063042
- Rebischung P, Altamimi Z, Ray J, Garayt B (2016) The IGS contribution to ITRF2014. *J Geod* 90:611–630. doi: 10.1007/s00190-016-0897-6
- Rodríguez-Pascua MA, Sánchez N, Pérez-López R, et al (2015) Análisis De La Deformación Frágil En Las Islas De Tenerife Y Lanzarote (Islas Canarias, España). Resultados Preliminares. Una visión Glob del Cuaternario El Hombre como condicionante los procesos geológicos 146–149.
- Romero-Ruiz C, García-Cacho L, Araña V, et al (2000) Submarine volcanism surrounding Tenerife, Canary Islands: Implications for tectonic controls, and oceanic shield forming processes. *J Volcanol Geotherm Res* 103:105–119. doi: 10.1016/S0377-0273(00)00218-3
- Rousseeuw PJ (1987) Silhouettes: A graphical aid to the interpretation and validation of cluster analysis. *J Comput Appl Math* 20:53–65. doi: 10.1016/0377-0427(87)90125-7
- Samsonov S, Tiampo K, Gonzalez PJ, et al (2008) Surface deformation studies of Tenerife Island, Spain from joint GPS-DInSAR observations. *Proc 2008 2nd Work USE Remote Sens Tech Monit Volcanoes Seism Areas, USEReST 2008* 1–6. doi: 10.1109/USEREST.2008.4740337
- Sánchez-Alzola A, Martí J, García-Yeguas A, Gil AJ (2016) Subsidence and current strain patterns on Tenerife Island (Canary Archipelago, Spain) derived from continuous GNSS

- time series (2008–2015). *J Volcanol Geotherm Res* 327:240–248. doi: 10.1016/j.jvolgeores.2016.08.006
- Scherneck H-G, Bos MS (2002) Ocean tide and atmospheric loading. *IVS 2002 Gen Meet Proc* 205–214.
- Sevilla MJ, Martin MD, Camacho AG (1986) Data analysis and adjustment of the first geodetic surveys in the Caldera of Teide, Tenerife, Canary Islands. *Tectonophysics* 130:213–234. doi: 10.1016/0040-1951(86)90113-7
- Sevilla MJ, Romero P (1991) Ground deformation control by statistical analysis of a geodetic network in the caldera of Teide. *J Volcanol Geotherm Res* 47:65–74. doi: 10.1016/0377-0273(91)90101-5
- Teza G, Pesci A, Galgaro A (2008) Grid_strain and grid_strain3: Software packages for strain field computation in 2D and 3D environments. *Comput Geosci* 34:1142–1153. doi: 10.1016/j.cageo.2007.07.006
- Tizzani P, Manconi A, Zeni G, et al (2010) Long-term versus short-term deformation processes at Tenerife (Canary Islands). *J Geophys Res* 115:B12412. doi: 10.1029/2010JB007735
- Vieira R, Toro C, Araña V (1986) Microgravimetric survey in the Caldera of Teide, Tenerife, Canary Islands. *Tectonophysics* 130:249–257. doi: 10.1016/0040-1951(86)90115-0
- Walter T, Schmincke H-U (2002) Rifting, recurrent landsliding and Miocene structural reorganization on NW-Tenerife (Canary Islands). *Int J Earth Sci* 91:615–628. doi: 10.1007/s00531-001-0245-8
- Williams SDP (2008) CATS: GPS coordinate time series analysis software. *GPS Solut* 12:147–153. doi: 10.1007/s10291-007-0086-4
- Zumberge JF, Heftin MB, Jefferson D, et al (1997) Precise point positioning for the efficient and robust analysis of GPS data from large networks. *J Geophys Res* 102:5005–5017. doi: 10.1029/96JB03860





2006

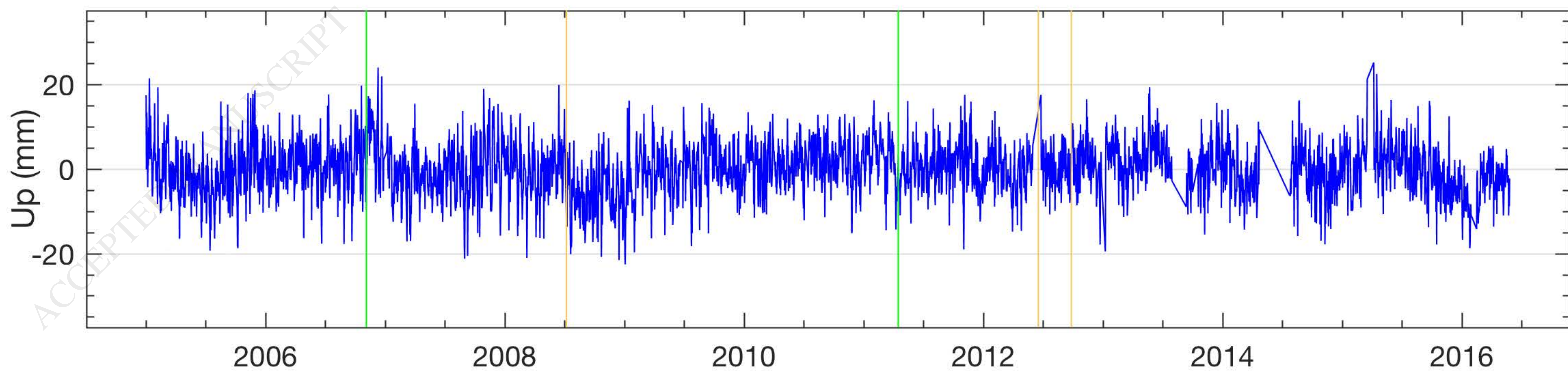
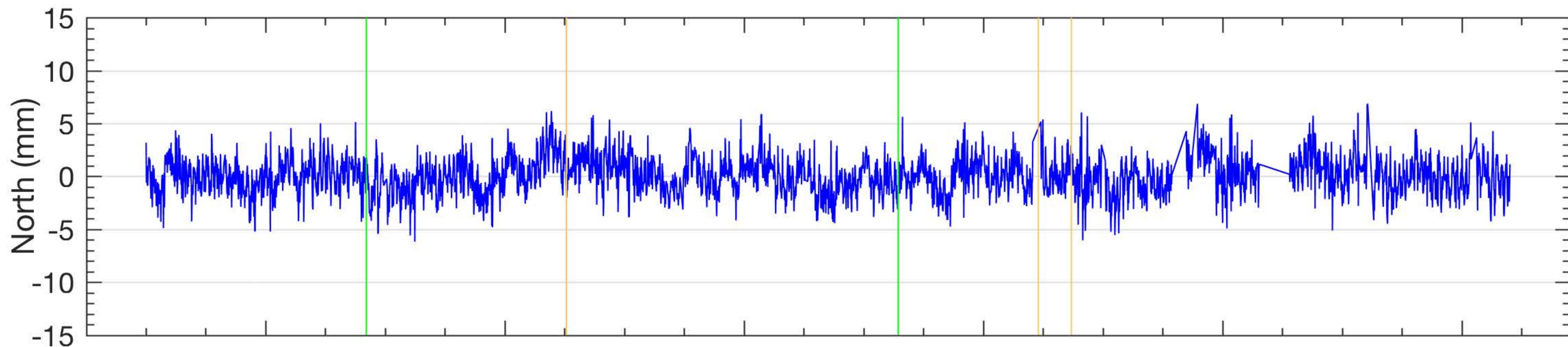
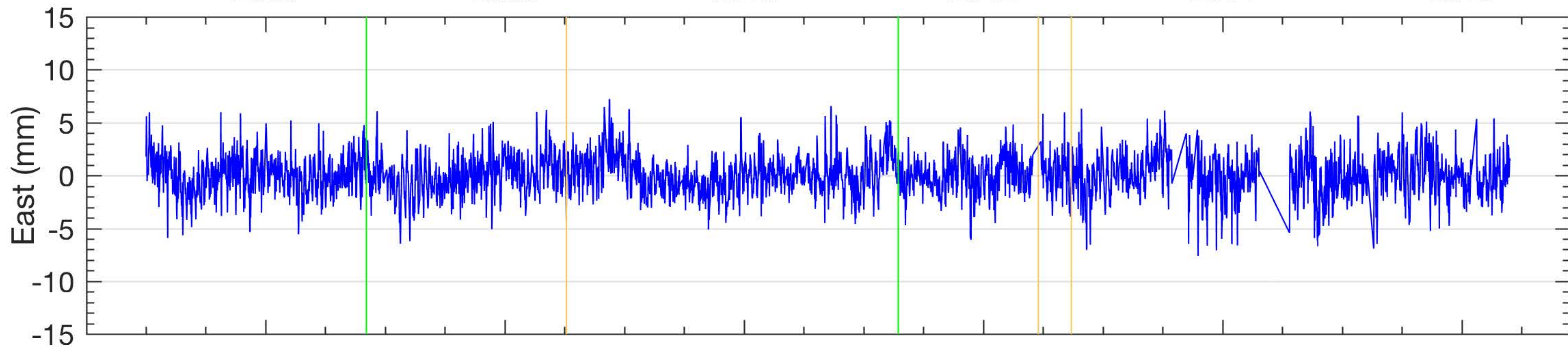
2008

2010

2012

2014

2016



2006

2008

2010

2012

2014

2016

325000

350000

375000

0 10 20 km

3150000

3150000

3125000

3125000

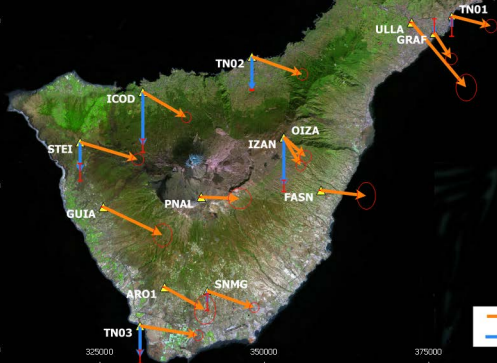
3100000

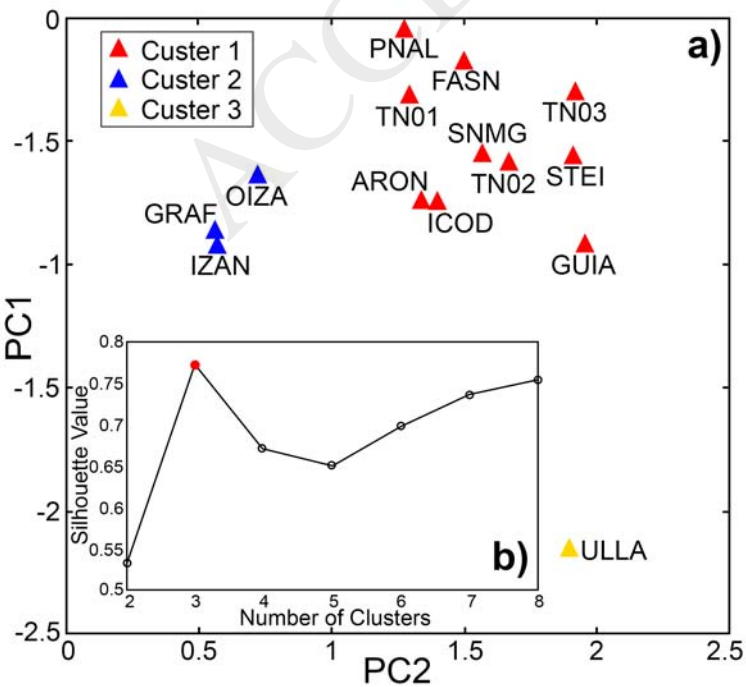
325000

350000

375000

3100000





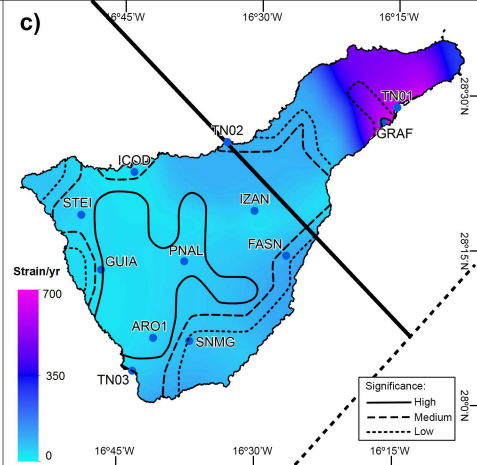
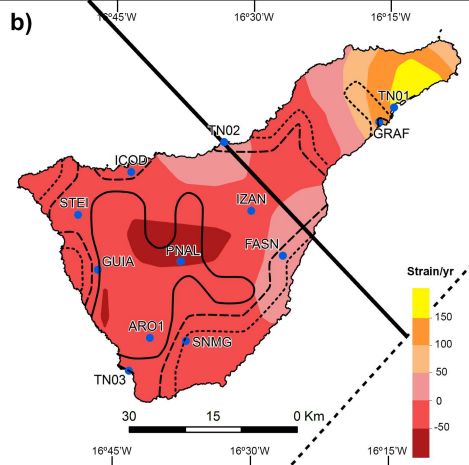
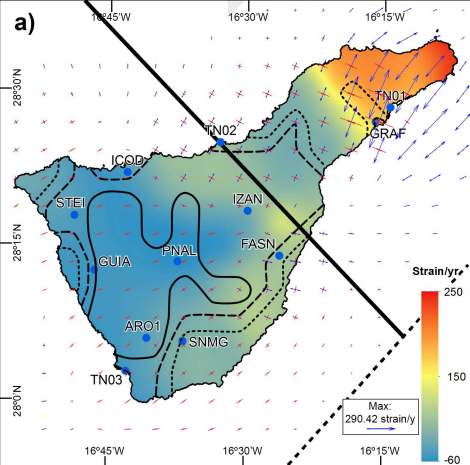


Table 1. Geographical coordinates (ITRF2008), first and final date of data, easting, northing and vertical velocities (mm/y) with respect to the ITRF2008 reference frame with uncertainties and residuals after correction from the NNR-Morvel56 Nubia Euler pole (dV_{E_Euler} and dV_{N_Euler}) for cGNSS and CGNSS stations.

cGNSS											
Site	Lon (deg)	Lat (deg)	Initial date	Final date	V_E (mm/y)	σ_E (mm/y)	V_N (mm/y)	σ_N (mm/y)	dV_{E_Euler} (mm/y)	dV_{N_Euler} (mm/y)	
ARO1	-16.681	28.1007	2005.297	2013.44	16.14	0.50	16.45	0.90	1.34	-0.75	
FASN	-16.441	28.2362	2005.244	2013.46	16.30	0.37	17.02	0.79	1.50	-0.18	
GUIA	-16.778	28.2094	2006.188	2013.46	16.66	0.40	16.27	0.56	1.96	-0.93	
PNAL	-16.627	28.2249	2005.245	2013.45	16.07	0.57	17.15	0.46	1.27	-0.05	
ULLA	-16.304	28.4677	2005.243	2013.44	16.51	0.46	15.15	0.78	1.81	-2.15	

CGNSS												
Site	Lon (deg)	Lat (deg)	Initial date	Final date	V_E (mm/y)	σ_E (mm/y)	V_N (mm/y)	σ_N (mm/y)	V_U (mm/y)	σ_U (mm/y)	dV_{E_Euler} (mm/y)	dV_{N_Euler} (mm/y)
GRAF	-16.268	28.4538	2010.162	2015.103	15.26	0.15	16.44	0.14	0.22	0.49	0.56	-0.86
ICOD	-16.719	28.3678	2005.246	2015.103	16.14	0.10	16.36	0.12	-1.78	0.43	1.44	-0.84
IZAN	-16.500	28.3081	2008.171	2015.103	15.26	0.11	16.27	0.12	-1.60	0.37	0.56	-0.93
OIZA	-16.500	28.3085	2005.244	2010.165	15.42	0.16	16.55	0.27	-1.94	0.55	0.72	-0.65
SNMG	-16.615	28.0965	2011.001	2015.103	16.36	0.10	16.65	0.11	-0.37	0.41	1.56	-0.55
STEI	-16.816	28.2977	2010.162	2015.103	16.61	0.16	16.53	0.15	-0.99	0.57	1.91	-0.57
TN01	-16.241	28.4772	2009.115	2015.103	16.00	0.17	16.97	0.20	-0.36	0.62	1.30	-0.33
TN02	-16.551	28.4183	2009.155	2015.103	16.37	0.14	16.61	0.14	-1.10	0.30	1.67	-0.59
TN03	-16.719	28.0472	2009.155	2015.103	16.72	0.11	16.89	0.12	-1.03	0.45	1.92	-0.31

Table 2. East and north velocity values from CGNSS stations for the local reference frame.

Station	East (mm/year)	North (mm/year)
ALAJ	15.8	16.6
GRAF	16.0	16.9
LPAL	16.1	16.5
MAS1	16.5	17.3
Average velocity	16.1	16.8

ACCEPTED MANUSCRIPT